Environ. Sci. Technol. 1993, 27, 2517-2522

Photochemistry of Aqueous Iron(III)–Polycarboxylate Complexes: Roles in the Chemistry of Atmospheric and Surface Waters

Bruce C. Faust*,† and Richard G. Zepp*,‡

Environmental Chemistry Laboratory, School of the Environment, Duke University, Durham, North Carolina 27708, and Environmental Research Laboratory, U.S. Environmental Protection Agency, Athens, Georgia 30605

Photochemical redox reactions of Fe(III) complexes of polycarboxylates (*e.g.*, citrate, malonate, oxalate) occur on time scales of minutes in sunlight and are potentially important sources of Fe(II), $^{\bullet}O_2^-/HO_2^{\bullet}$, H_2O_2, and $^{\bullet}OH$ in atmospheric water drops and surface waters. Quantum yields for Fe(II) formation, determined from experiments and equilibrium speciation calculations, are (i) 0.28 for $Fe(OH)(citrate)^-$ at 436 nm, (ii) 0.027 for $Fe(malonate)_2^-$ at 366 nm, and (iii) 1.0 for $Fe(oxalate)_2^-$ and 0.6 for $Fe(oxalate)_3^{3-}$ at 436 nm. Competitive reactions of O_2 and Fe(III) with the polycarboxylate radicals and/or the carbon-centered radicals derived from decarboxylation, as well as the speciation of Fe(II) and Fe(III), affect the experimental quantum yields of Fe(II) formation.

Introduction

The carboxylate group [R-C(O)O$^-$] is one of the most common functional groups of the dissolved organic compounds present in natural waters (*1, 2*). Polycarboxylates (*i.e.*, molecules that have more than one carboxylate functional group), including citrate, malonate, and oxalate, are common constituents of precipitation (*3, 4*), fog (*4*), urban (*5, 6*) and remote (*7*) tropospheric aerosols, surface waters (*1, 8*), and soil solutions (*9*). Polycarboxylates form strong complexes with Fe^{3+} that undergo rapid photochemical reactions in sunlight (*10*).

Photolysis of Fe(III)–polycarboxylates affects the speciation of iron in atmospheric and surface waters, which in turn affects numerous iron-dependent biogeochemical processes (*10*). Sunlight photolysis of naturally occurring Fe(III)–carboxylate moieties is also responsible for the iron-mediated photochemical production of CO_2 and consumption of O_2 in humic-colored natural waters (*11*). Esterification of carboxylate groups in the natural organic matter decreased oxygen consumption rates by 50% (*11*).

Since the 1950s, numerous investigations have found that Fe(III)–oxalate complexes photolyze with high efficiency (*10–18*, and references cited therein). Little is known, however, about the effect of oxygen on the experimental quantum yields of Fe(II) formation for this reaction. Moreover, scant information is available on the photolysis of other Fe(III)–polycarboxylates for the conditions of pH and of iron and carboxylate concentrations that are more typical of natural aquatic environments (*14*). Thus, the objectives of this work were to determine the quantum yields of Fe(II) formation for several Fe(III)–polycarboxylates and to examine the effects of iron speciation and oxygen on the experimental quantum yields of Fe(II).

* Correspondence may be addressed to either author.
† Duke University.
‡ U.S. Environmental Protection Agency.

Conceptual Model

Figure 1 illustrates a reaction scheme that is consistent with observations from this study. Absorption of a photon by an Fe(III)–polycarboxylate species initiates the formation of short-lived intermediates (*15, 16*) that ultimately yield Fe(II) and a free polycarboxylate radical outside of the solvent cage (Figure 1). Several competing processes can affect the fate of the polycarboxylate radical (Figure 1): (i) back-reaction with Fe(II) to re-form Fe(III) (not shown in Figure 1); (ii) reaction with O_2 to form $^{\bullet}O_2^-/HO_2^{\bullet}$; (iii) reduction of another Fe(III)–polycarboxylate species, which is rapid for reaction of $C_2O_4^{\bullet-}$ with Fe(III)–oxalate species [$k > 5 \times 10^7\ M^{-1}\ s^{-1}$ (*15, 16*)]; or (iv) decarboxylation, which is a rapid process for $C_2O_4^{\bullet-}$ [half-life $\approx 0.3\ \mu s$ (*19*)], to form carbon-centered radicals. Carbon-centered radicals also react at near-diffusion-controlled rates with O_2 and Fe(III)–carboxylate species (*20, 21*).

A very important consideration is the competition between O_2 and Fe(III) species for the polycarboxylate radical ($RCOO^{\bullet n-}$) and the carbon-centered radical (>C$^{\bullet}$) derived therefrom (*12*). If the $RCOO^{\bullet n-}$ and >C$^{\bullet}$ radicals react with Fe(III), then additional Fe(II) is formed; however, if they react with O_2, then a sequence of oxidants ($^{\bullet}O_2^-/HO_2^{\bullet}$, H_2O_2, $^{\bullet}OH$, $ROO^{\bullet}$, ROOH) are formed, each of which can oxidize Fe(II) (Figure 1). As will be seen, this can reduce substantially the experimental quantum yield for Fe(II) formation, relative to the Fe(II) quantum yield for the primary photochemical step.

Experimental and Computational Methods

Except where noted, all reagents, purified water, apparatus and equipment, analytical and experimental procedures and conditions, protocols for preparation and irradiation of solutions, kinetic analyses, and speciation computations were identical to those previously described (*17*). The solution composition and speciation calculations were previously described (298 K, 0.01 M ionic strength, 1 atm; see Tables I and III of ref 17); the only differences being that scavengers and probe molecules (*e.g.*, 1-octanol, 2-methyl-2-propanol, nitrobenzene, anisole, etc.) were not present in these solutions. More information regarding the stoichiometries and stability constants (*22–28*) of species considered in the equilibrium speciation computations are given in Table I. All ionic strength corrections were made using the Davies equation (*29*). All Fe(III)–polycarboxylate solutions were freshly prepared within 1 h of the time of irradiation.

Monochromatic illumination utilized a Schoeffel Reaction Chemistry System equipped with a monochromator (*17*). Solutions were either saturated with air or purged with argon prior to irradiation. Solutions were irradiated in stoppered rectangular quartz cuvettes that were stirred continuously with a Teflon-coated magnetic stir bar.

Potassium ferrioxalate, synthesized and recrystallized as described elsewhere (*30*), was used as a chemical

0013-936X/93/0927-2517$04.00/0 © 1993 American Chemical Society

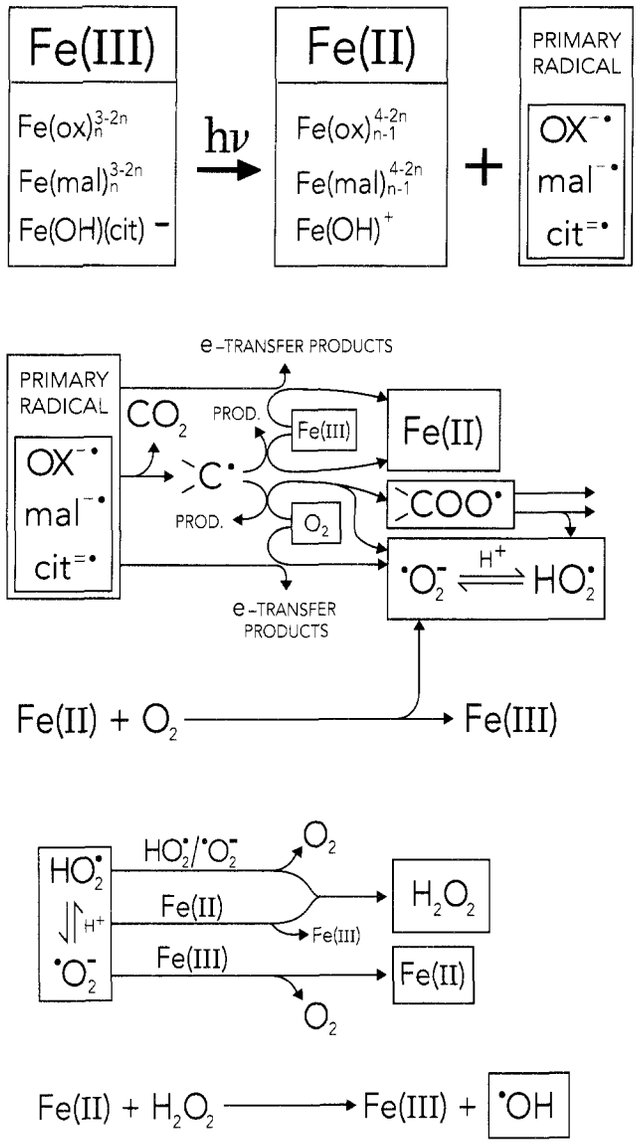

Figure 1. Reaction scheme for the photolysis of Fe(III) complexes of polycarboxylates (oxalate^{2-} = ox^{2-}, malonate^{2-} = mal^{2-}, citrate^{3-} = cit^{3-}). The symbol >C• represents the carbon-centered radical derived from the decarboxylation of the polycarbonate radical, or $CO_2^{\bullet-}$ in the case of oxalate. Note that not all polycarboxylate-derived >C• will necessarily form $^{\bullet}O_2^-$ upon reaction with O_2; reaction of some >C• with O_2 could form organic peroxyl radicals (>COO•, or more generally, ROO•) that could form organic peroxides rather than H_2O_2.

actinometer; 0.15 M $K_3Fe(C_2O_4)_3 \cdot 3H_2O$ in air-saturated aqueous solutions of 0.10 M H_2SO_4 was used for all experiments (*30*). Under conditions of nearly complete light absorption at the photolysis wavelength (λ), I_λ (einstein L^{-1} s^{-1}) was determined from $I_\lambda = (d[Fe(II)]/dt)/\Phi_{Fe(II),\lambda}$, where $\Phi_{Fe(II),\lambda}$ is the quantum yield for Fe(II) formation from solutions of $K_3Fe(C_2O_4)_3$, and $d[Fe(II)]/dt$ is determined from the slope of a linear plot of [Fe(II)] versus irradiation time (*30*). No detectable Fe(II) formation occurred in actinometer solutions or in Fe(III)–polycarboxylate solutions kept in the dark for the time period corresponding to the duration of irradiation of the solution. Values of $\Phi_{Fe(II),\lambda}$ for solutions of $K_3Fe(C_2O_4)_3$ that were used in all calculations were $\Phi_{Fe(II),366} = 1.15$ and $\Phi_{Fe(II),436} = 1.01$ (*30*).

Rates of Fe(II) photoformation from Fe(III)–polycarboxylate solutions were determined from the initial slope of a plot of [Fe(II)] versus irradiation time. Irradiation

Table I. Species Composition Matrix: Components and Their Corresponding Stoichiometric Coefficients and Equilibrium Formation Constant for Each Species[a]

	components[b]								
species	Fe^{3+}	Fe^{2+}	ox^{2-}	mal^{2-}	cit^{3-}	PO_4^{3-}	H^+	$\log_{10}\beta$	ref
$Fe(OH)^{2+}$	1						−1	−2.2	22
$Fe(OH)_2^+$	1						−2	−7.1[c]	23
$Fe(OH)_3$(am)	1						−3	−3.2	22
$Fe_2(OH)_2^{4+}$	2						−2	−2.9	22
$Fe(OH)_4^-$	1						−4	−21.6	22
$Fe(OH)^+$		1					−1	−9.5	22
$Fe(ox)^+$	1		1					9.4	22
$Fe(ox)_2^-$	1		2					16.2	22
$Fe(ox)_3^{3-}$	1		3					20.4	22
$Fe(Hox)^{2+}$	1		1				1	9.5	22
$Fe(ox)^0$		1	2					4.3	22
$Fe(ox)_2^{2-}$		1	2					6.4	22
$Fe(mal)^+$	1			1				9.3	24
$Fe(mal)_2^-$	1			2				15.5	24
$Fe(mal)_3^{3-}$	1			3				18.4	24
$Fe(mal)^0$		1		1				3.4	24
$Fe(mal)_2^{2-}$		1		2				4.4	24
$Fe(cit)^0$	1				1			13.2	25
$Fe(Hcit)^+$	1				1		1	14.4	25
$Fe(OH)(cit)^-$	1				1		−1	10.3	25
$Fe(cit)^-$		1			1			6.1	25
$Fe(Hcit)^0$		1			1		1	10.1[d]	25
$Fe(H_2cit)^+$		1			1		2	13.9	26
$Fe(Hcit)(cit)^{3-}$		1			2		1	13.9[e]	27
$Fe(PO_4)$(am)	1					1		23	28
$Fe(HPO_4)^+$	1					1	1	22.5	22
$Fe(H_2PO_4)^{2+}$	1					1	2	24.0	22
$Fe_3(PO_4)_2$(s)		3				2		36.0	22
$Fe(HPO_4)^0$		1				1	1	16.0	22
$Fe(H_2PO_4)^+$		1				1	2	22.3	22

[a] All thermodynamic data are for 298 K, 1 atm, with ionic strength → 0. {species} = β{component 1}^{i}{component 2}^{j}{component 3}^{k} ..., where { } signifies the molar activity of the species/component; i, j, k, ... are stoichiometric coefficients for the corresponding component; and β is the equilibrium constant for formation of the species. pK_a values (*22*): (1) 1.25 and 4.27 for H_2ox, (2) 2.85 and 5.70 for H_2mal, (3) 3.13, 4.76, and 6.40 for H_3cit, and (4) 2.15, 7.20, and 12.35 for H_3PO_4. $\{H^+\}\{OH^-\} = 10^{-14.00}$. The activity (mole fraction) of liquid H_2O and all solid phases is 1 for these calculations. Blank entries in the table are zero. This information was also used to calculate the speciation for ref 17. [b] ox^{2-} = oxalate^{2-}; mal^{2-} = malonate^{2-}; cit^{3-} = citrate^{3-}. [c] Value of −5.7 (*22*) was also used in sensitivity calculations (*17*). [d] Value of 10.8 (*22*) was also used in sensitivity calculations (*17*). [e] 310 K.

times were typically <10 min and were always <30 min. It should be noted, however, that for air-saturated solutions even these initial rates were probably decreased by re-oxidation of Fe(II) (*e.g.*, by $^{\bullet}O_2^-/HO_2^{\bullet}$).

Values of $\Phi_{Fe(II),\lambda}$ for Fe(III)–polycarboxylate solutions were determined from $\Phi_{Fe(II),\lambda} = (d[Fe(II)]/dt)/I_{abs,\lambda}$, where $I_{abs,\lambda} = I_\lambda(1 - 10^{-A_\lambda})$. For the conditions of our experiments, the absorbance (A_λ) of the Fe(III)–polycarboxylate solutions was dominated by the Fe(III)–polycarboxylate species. An experimental Fe(III)-based decadic molar absorptivity (M^{-1} cm^{-1}) for the solution, $\epsilon_{Fe(III),\lambda}$, is defined as $\epsilon_{Fe(III),\lambda} = A_\lambda/\{[Fe(III)](\text{path length})\}$.

Results and Discussion

Iron(II) Quantum Yields for Fe(III)–Polycarboxylates: Argon-Saturated Solutions. Table II summarizes results for the Fe(III)–citrate system for a pH range (pH 4–6) that is typical of natural waters having high concentrations of carboxylic acids (*1*, *2*). Table II shows that the experimental quantum yield for Fe(II) formation ($\Phi_{Fe(II),436}$) decreases slightly: (i) from 0.28 at pH 4 to 0.21 at pH 6 and (ii) from 0.28 at 1:1 Fe(III)/citrate stoichi-

Table II. Effects of pH and Citrate Concentration on the Experimental Quantum Yields for Fe(II) Formation at 436 nm ($\Phi_{Fe(II),436}$) in the Fe(III)–Citrate System[a]

pH	total [citrate] (mM)	$\Phi_{Fe(II),436}$
4.0[b]	0.10	0.28
5.0[b]	0.10	0.25
6.0[b]	0.10	0.21
4.0[c]	0.10	0.28
4.0[c]	0.50	0.25
4.0[c]	1.00	0.24

[a] [Fe(III)] = 0.10 mM; ionic strength 10 mM; temperature 298 K; argon purged. [b] Total [orthophosphate] = 5.0 mM. [c] pH adjusted by dropwise addition of an aqueous bicarbonate solution; orthophosphate was not added.

ometry to 0.24 at 1:10 Fe(III)/citrate stoichiometry. The equilibrium Fe(III) speciation is predicted to be the same for all of the citrate experiments listed in Table II [93% $Fe(OH)(citrate)^-$, 6.6% $Fe(citrate)^0$]. Although we do not have a definitive explanation for the variations in Fe(II) quantum yields despite predicted invariance in Fe(III) speciation for the Fe(III)–citrate experiments, it is conceivable that another Fe(III)–citrate species could be formed at higher pH and/or total citrate concentrations. The limiting quantum yield is $\Phi_{Fe(II),436} = 0.28$ for both the pH and total citrate concentration dependence studies (Table II), and this is assigned to $Fe(OH)(citrate)^-$.

For the malonate system ([Fe(III)] = 0.10 mM, total [malonate] = 5.0 mM, pH = 4.0, 0.01 M ionic strength, 298 K), an experimental quantum yield for Fe(II) formation at 366 nm of $\Phi_{Fe(II),366} = 0.027$ was determined in argon-saturated solutions, based on a value of $\epsilon_{Fe(III),366} = 8.0\ M^{-1}\ cm^{-1}$. For these conditions, the calculated equilibrium speciation suggests that the percentage of total Fe(III) present as a given species is <0.001% for $FeOH^{2+}$, <1% for $Fe(malonate)^+$, 87% for $Fe(malonate)_2^-$, and 13% for $Fe(malonate)_3^{3-}$. For several reasons it is highly likely that the photochemistry of this malonate system is dominated by $Fe(malonate)_2^-$. One, the equilibrium concentration of $Fe(malonate)_2^-$ is calculated to be >100 times that of $Fe(malonate)^+$ and 6.7 times that of $Fe(malonate)_3^{3-}$. Two, by analogy with Fe(III) complexes of *o*-dihydroxybenzenes and salicylates (*31*), it is highly likely that the peak of the ligand-to-metal charge-transfer transition for $Fe(malonate)_3^{3-}$ is at a shorter wavelength than that of $Fe(malonate)_2^-$. Since our observations indicate that both peaks are located below 366 nm, the molar absorptivity at 366 nm of $Fe(malonate)_2^-$ is probably greater than that of $Fe(malonate)_3^{3-}$. This behavior has been observed for the corresponding 1:2 and 1:3 Fe(III)–oxalate complexes (*vide infra*). Three, it is also probable that increasing negative charge on the central Fe(III) ion makes electron transfer from the malonate-centered orbital to the Fe(III)-centered orbital less favorable for $Fe(malonate)_3^{3-}$ than for $Fe(malonate)_2^-$ (*31*); therefore, the quantum yield of $Fe(malonate)_3^{3-}$ is probably not larger than that of $Fe(malonate)_2^-$. For the aforementioned reasons, the experimental quantum yield of $\Phi_{Fe(II),366} = 0.027$ is assigned to $Fe(malonate)_2^-$.

It is noteworthy that the quantum yield for Fe(II) formation of $Fe(malonate)_2^-$ at 366 nm is only 2.7% of that for $Fe(oxalate)_2^-$ at 436 nm (*vide infra*). Several factors could contribute to this large difference in quantum yields, including variability in the relative rates of different polycarboxylate radical reactions [*e.g.*, decarboxylation and recombination with Fe(II)] as well as differences in the photoinduced ligand-to-metal charge transfer of the Fe(III) complexes. Sorting out the different contributing factors was beyond the scope of this study.

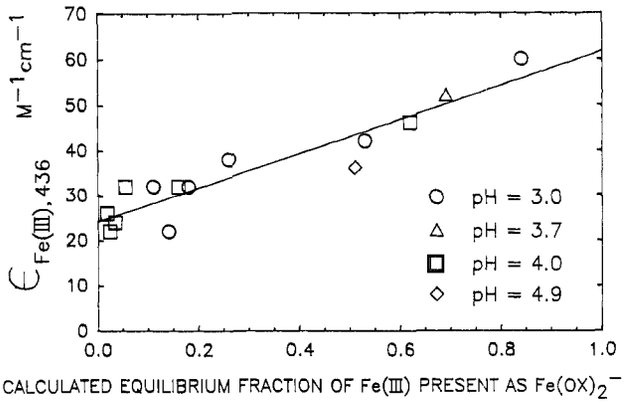

Figure 2. Measured experimental Fe(III)-based decadic molar absorptivity at 436 nm, $\epsilon_{Fe(III),436}$, for each Fe(III)–oxalate solution versus the calculated equilibrium fraction of Fe(III) present as $Fe(ox)_2^-$ for the same solution. The least-squares linear regression of the data is given by the line. The right intercept ($f_{1:2} = 1$) and left intercept ($f_{1:2} = 0$, $f_{1:3} = 1$) are the decadic molar absorptivities (value ± SE) of $Fe(ox)_2^-$ ($\epsilon_{1:2,436} = 62 \pm 6\ M^{-1}\ cm^{-1}$) and $Fe(ox)_3^{3-}$ ($\epsilon_{1:3,436} = 24 \pm 4\ M^{-1}\ cm^{-1}$), respectively. See eq 1 and the text for further explanation.

For the conditions of the Fe(III)–oxalate experiments (*17*), the absorbance and photochemistry at 436 nm is dominated by $Fe(oxalate)_2^-$ and $Fe(oxalate)_3^{3-}$; the sum of the concentrations of $Fe(oxalate)_2^-$ and $Fe(oxalate)_3^{3-}$ is calculated to be much larger than the sum of concentrations of all other Fe(III) species (more than 5000 times larger for half of the solutions and more than 100 times larger for all but one of the solutions). In other words, the sum of the calculated equilibrium fractions of Fe(III) present as $Fe(oxalate)_2^-$ ($f_{1:2}$) and $Fe(oxalate)_3^{3-}$ ($f_{1:3}$) are approximately unity ($f_{1:2} + f_{1:3} \simeq 1$).

Figure 2 shows the linear relationship between the experimental Fe(III)-based decadic molar absorptivities and the calculated equilibrium fraction of Fe(III) present as $Fe(oxalate)_2^-$. This linear relationship is consistent with the view that the absorbance of these Fe(III)–oxalate solutions is dominated by $Fe(oxalate)_2^-$ and $Fe(oxalate)_3^{3-}$. Equation 1 is consistent with this observed linear relationship and relates the experimental Fe(III)-based molar absorptivity to the molar absorptivities of $Fe(oxalate)_2^-$ and $Fe(oxalate)_3^{3-}$:

$$\epsilon_{Fe(III),436} \simeq (\epsilon_{1:3,436}) + (\epsilon_{1:2,436} - \epsilon_{1:3,436})(f_{1:2}) \qquad (1)$$

where $\epsilon_{1:2,436}$ and $\epsilon_{1:3,436}$ are the decadic molar absorptivities ($M^{-1}\ cm^{-1}$) at 436 nm of $Fe(oxalate)_2^-$ and $Fe(oxalate)_3^{3-}$, respectively. For these experiments, the molar absorptivities $\epsilon_{1:2,436}$ and $\epsilon_{1:3,436}$ were determined from the intercepts of Figure 2; the calculated values are $\epsilon_{1:2,436} = 62 \pm 6$ ($f_{1:2} = 1$, right intercept) and $\epsilon_{1:3,436} = 24 \pm 4$ ($f_{1:2} = 0$, $f_{1:3} = 1$, left intercept).

A similar analysis was carried out for the photochemistry of the Fe(III)–oxalate solutions. Figure 3 illustrates that the product of the experimental quantum yield and experimental Fe(III)-based molar absorptivity is linearly related to the fraction of Fe(III) present as $Fe(oxalate)_2^-$. This linear relationship is consistent with the view that photoformation of Fe(II) in these solutions is dominated by $Fe(oxalate)_2^-$ and $Fe(oxalate)_3^{3-}$. Equation 2 is consistent with this observed linear relationship and relates

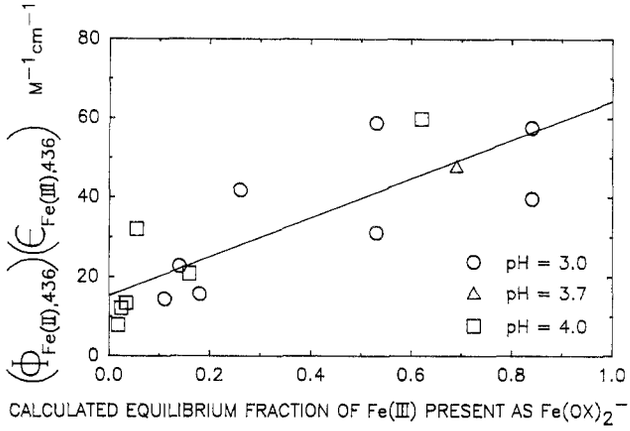

Figure 3. Product of the independently measured experimental quantum yield for Fe(II) formation ($\Phi_{Fe(II),436}$) and the experimental Fe(III)-based decadic molar absorptivity ($\epsilon_{Fe(III),436}$) at 436 nm for each Fe(III)–oxalate solution versus the calculated equilibrium fraction of Fe(III) present as $Fe(ox)_2^-$ for the same solution. The least-squares linear regression of the data is given by the line. The right intercept ($f_{1:2}$ = 1) and left intercept ($f_{1:2}$ = 0, $f_{1:3}$ = 1) are the quantities (value ± SE) for the individual complexes, $(\Phi_{Fe(II),436,1:2})(\epsilon_{1:2,436})$ = 64 ± 14 and $(\Phi_{Fe(II),436,1:3})(\epsilon_{1:3,436})$ = 15 ± 11 M^{-1} cm^{-1}, respectively. See eq 2 and the text for further explanation.

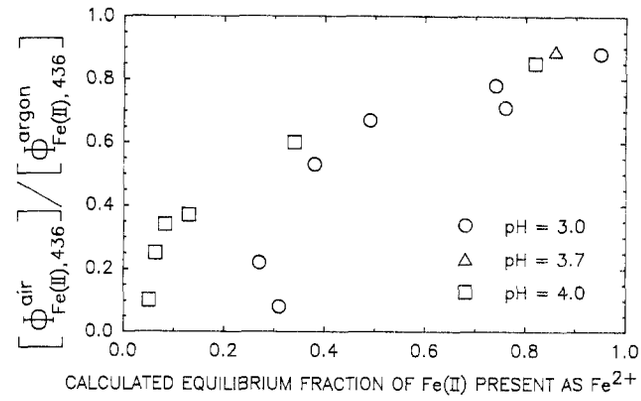

Figure 4. Measured experimental quantum yield for Fe(II) formation at 436 nm for each air-saturated Fe(III)–oxalate solution divided by that for the same Fe(III)–oxalate solution after purging with argon versus the calculated equilibrium fraction of Fe(II) present as Fe^{2+} for the same solution.

the experimental quantities to the fundamental quantum yields and molar absorptivities of $Fe(oxalate)_2^-$ and $Fe(oxalate)_3^{3-}$:

$$(\Phi_{Fe(II),436})(\epsilon_{Fe(III),436}) \simeq (\Phi_{Fe(II),436,1:3})(\epsilon_{1:3,436}) + [(\Phi_{Fe(II),436,1:2})(\epsilon_{1:2,436}) - (\Phi_{Fe(II),436,1:3})(\epsilon_{1:3,436})](f_{1:2}) \quad (2)$$

where $\Phi_{Fe(II),436,1:2}$ and $\Phi_{Fe(II),436,1:3}$ are the quantum yields for Fe(II) formation at 436 nm of $Fe(oxalate)_2^-$ and $Fe(oxalate)_3^{3-}$, respectively. Using the information given in Figure 2 and the molar absorptivities ($\epsilon_{1:2,436}$ and $\epsilon_{1:3,436}$) given previously (Figure 2), we calculated (eq 2) quantum yields for Fe(II) formation at 436 nm to be $\Phi_{Fe(II),436,1:2}$ = 1.0 ± 0.25 for $Fe(oxalate)_2^-$ and $\Phi_{Fe(II),436,1:3}$ = 0.60 ± 0.46 for $Fe(oxalate)_3^{3-}$. It should be emphasized that these quantum yields are not those of the primary photochemical process, but that they also include contributions from secondary reactions involving the oxalate radical.

Oxygen Effects on Experimental Fe(II) Quantum Yields. For the Fe(III)–oxalate system, the experimental quantum yields for Fe(II) formation in air-saturated solutions were substantially lower, by as much as a factor of 10, than those for identical argon-purged solutions. The effect of air is attributed to the reaction of aqueous O_2 (*ca.* 0.25 mM in air-saturated aqueous solutions) with $C_2O_4^{\bullet-}$ and $CO_2^{\bullet-}$ to form $^{\bullet}O_2^-/HO_2^{\bullet}$. Reactions of $C_2O_4^{\bullet-}/CO_2^{\bullet-}$ with O_2 decrease the experimental quantum yield for Fe(II) formation in two ways (see Figure 1 for more detail). One, O_2 competes with Fe(III) for $C_2O_4^{\bullet-}/CO_2^{\bullet-}$, which limits the formation of additional Fe(II) from reactions of $C_2O_4^{\bullet-}/CO_2^{\bullet-}$ with Fe(III). Two, more importantly, the formation of $^{\bullet}O_2^-/HO_2^{\bullet}$ is the first step in generating a series of oxidants (*e.g.*, $HO_2^{\bullet}$, H_2O_2, $^{\bullet}OH$) that can oxidize Fe(II), as shown in Figure 1.

The decrease in experimental Fe(II) quantum yields in air-saturated solutions cannot be attributed to thermal oxidation of Fe(II) by O_2 because micromolar concentrations of Fe(II) added to air-saturated unirradiated Fe(III)–oxalate solutions were oxidized on time scales that were slow [half-life of Fe(II) ≈ 30 min] compared to the time scales of these photolysis experiments (10 min) (*32*). Thus, other oxidants, such as $^{\bullet}O_2^-/HO_2^{\bullet}$ in the early stages of the reaction and also H_2O_2 and $^{\bullet}OH$ later in the reaction, probably re-oxidized the photoformed Fe(II). Re-oxidation of Fe(II) lowered the experimental quantum yield for Fe(II) formation. Addition of H_2O_2 to preirradiated Fe(III)–oxalate solutions resulted in the rapid oxidation of Fe(II) [half-life < 1 min (*17*)].

The speciation of Fe(II) is expected to affect the rate of Fe(II) oxidation by H_2O_2 (*33*, *34*). For the oxalate system, the calculated equilibrium speciation of Fe(II) was dominated by Fe^{2+}, $Fe(oxalate)^0$, and $Fe(oxalate)_2^{2-}$; $FeOH^+$ represented less than 0.002% of the total Fe(II) in these oxalate solutions. Numerous studies (see Table I of ref 33) have found that H_2O_2 reacts 10–1000 times faster with Fe(II)–polycarboxylate complexes than with Fe^{2+}. Thus for air-saturated Fe(III)–oxalate solutions [which form H_2O_2 upon photolysis (*18*)], it is expected that as the fraction of Fe(II) present as Fe^{2+} increases, the rate of Fe(II) oxidation by H_2O_2 decreases, and correspondingly, the experimental quantum yield for Fe(II) formation increases. Figure 4 is consistent with this hypothesis and illustrates that the experimental quantum yields for Fe(II) formation in air-saturated Fe(III)–oxalate solutions approach the values of their corresponding argon-saturated solutions as the fraction of Fe(II) present as Fe^{2+} increases.

An important consideration in the formation of H_2O_2 (and other O_2-derived oxidants) is the competitive reactions of Fe(III) species and O_2 with $C_2O_4^{\bullet-}/CO_2^{\bullet-}$ (Figure 1). If $C_2O_4^{\bullet-}/CO_2^{\bullet-}$ reacts with Fe(III), then additional Fe(II) is formed: however, if $C_2O_4^{\bullet-}/CO_2^{\bullet-}$ reacts with O_2, then a "cascade" of oxidants (including H_2O_2) is formed which can oxidize Fe(II) (Figure 1). The Fe(III) speciation is expected to affect the competition between Fe(III) and O_2 for $C_2O_4^{\bullet-}/CO_2^{\bullet-}$ and, therefore, the experimental quantum yields for Fe(II) formation in air-saturated solutions. Specifically, it is likely that $C_2O_4^{\bullet-}$ and $CO_2^{\bullet-}$ will transfer an electron to $Fe(oxalate)_3^{3-}$ more slowly than they will to $Fe(oxalate)_2^-$ or $Fe(oxalate)^+$, due to electrostatic repulsion.

Thus in the Fe(III)–oxalate solutions, as the fraction of Fe(III) present as $Fe(oxalate)_3^{3-}$ increases, a greater fraction of $C_2O_4^{\bullet-}/CO_2^{\bullet-}$ reacts with O_2 rather than with Fe(III), and consequently the formation rates and concentrations of the O_2-derived oxidants (*e.g.*, H_2O_2) increase. This change in Fe(III) speciation accelerates the rates of

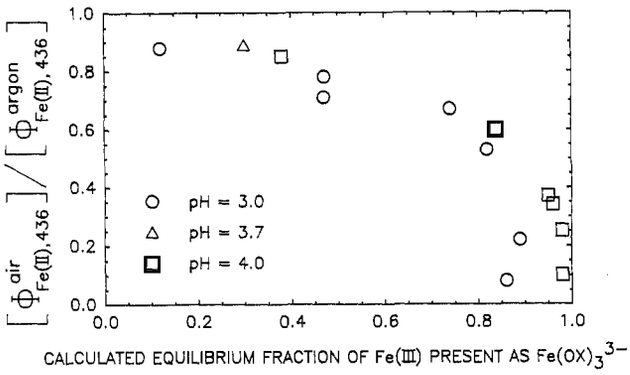

Figure 5. Measured experimental quantum yield for Fe(II) formation at 436 nm in air-saturated Fe(III)–oxalate solution divided by that for the same Fe(III)–oxalate solution after purging with argon versus the calculated equilibrium fraction of Fe(III) present as $Fe(ox)_3^{3-}$ for the same solution.

Fe(II) oxidation and lowers the experimental quantum yield for Fe(II) formation. Figure 5 is consistent with this hypothesis and shows that the experimental quantum yield for Fe(II) formation in air-saturated solution, relative to that for the identical argon-saturated solution, decreases as the calculated equilibrium fraction of Fe(III) present as $Fe(oxalate)_3^{3-}$ increases.

Significance to Atmospheric and Surface Waters. The half-lifes of Fe(III)–polycarboxylate species in sunlight (latitude 34° N, midday, June) are 0.2 min for $Fe(oxalate)^+/Fe(oxalate)_2^-$ (*18*, *35*), 5 min for $Fe(malonate)^+/Fe(malonate)_2^-$ (this work), and 0.9 min for $Fe(OH)(citrate)^-$ (this work). With half-lifes on the order of minutes, the photolysis of Fe(III)–polycarboxylates represents a potentially important daytime source of Fe(II) to atmospheric and surface waters and could easily account for much of the Fe(II) formation in many natural waters (*10*).

Photolysis of Fe(III)–polycarboxylates is a sink for the polycarboxylates and, through decarboxylation of the polycarboxylate radical, is a source of CO_2 to the system (Figure 1). The iron-mediated photomineralization of natural organic compounds has received little study (*11*) but could be an important mechanism for the cycling of carbon in natural waters having appreciable concentrations of dissolved organic carbon (DOC) and iron (*10*). Furthermore, in such natural waters, photoredox reactions of Fe(III)–polycarboxylates could represent a significant sink for dissolved O_2 (*11*).

The reduction of O_2 through photolysis of Fe(III)–polycarboxylates forms $^{\bullet}O_2^-/HO_2^{\bullet}$, which in turn forms H_2O_2 (Figure 1). Given the high photoreactivity of Fe(III)–polycarboxylates, their photolysis could represent an important source of H_2O_2 to some atmospheric and surface waters (*10*, *18*).

For atmospheric and surface waters having significant concentrations of Fe(III)–polycarboxylates, the simultaneous and rapid photoformation of Fe(II) and H_2O_2 could represent a significant thermal source of hydroxyl radical ($^{\bullet}OH$), through Fenton's reaction of Fe(II) with H_2O_2 (Figure 1). In this model, polycarboxylates have three important roles. One, polycarboxylates increase the concentration of dissolved Fe(III) because they form strong complexes with Fe^{3+}. Two, Fe(III)–polycarboxylates photolyze rapidly, which reduces Fe(III) to Fe(II) and simultaneously reduces O_2 to H_2O_2 (Figure 1). Three, H_2O_2 reacts much faster with Fe(II)–polycarboxylates than with Fe^{2+} (*33*); therefore, polycarboxylates apparently increase the rate of $^{\bullet}OH$ formation in the photo-Fenton reaction, because one $^{\bullet}OH$ is formed for every Fe(II) oxidized by H_2O_2 in irradiated Fe(III)–polycarboxylate solutions (*17*).

Finally, the results reported here are for the pH range 3.0–6.0, which is typical of atmospheric waters and of surface waters with high DOC concentrations. Depending on the exact conditions of a natural water (*e.g.*, pH, [Fe(III)], [DOC]), precipitation of ferrihydrite [amorphous $Fe(OH)_3$] could occur (*10*, *29*), and this would, of course, affect the photochemistry of the Fe(III) (*10*).

Acknowledgments

We thank D. L. Ceiler, J. M. Garraty, and G. Rosario for obtaining some of the kinetics data and M. Z. Hoffman for his useful comments. B.C.F. received support from the Atmospheric Chemistry Program of the U.S. National Science Foundation and from the Andrew W. Mellon Foundation.

Literature Cited

(1) Thurman, E. M. *Organic Geochemistry of Natural Waters*; Martinus Nijhoff, Dr. W. Junk: Dordrecht, 1985; pp 88–92, 295–299.
(2) Perdue, E. M.; Gjessing, E. T. *Organic Acids in Aquatic Ecosystems*; Wiley: New York, 1990.
(3) Likens, G. E.; Edgerton, E. S.; Galloway, J. N. *Tellus* **1983**, *35B*, 16–24.
(4) Kawamura, K.; Steinberg, S.; Kaplan, I. R. *Int. J. Environ. Anal. Chem.* **1985**, *19*, 175–188.
(5) Grosjean, D.; Van Cauwenberghe, K.; Schmid, J. P.; Kelley, P. E.; Pitts, J. N., Jr. *Environ. Sci. Technol.* **1978**, *12*, 313–317.
(6) Satsumabayashi, H.; Kurita, H.; Yokouchi, Y.; Ueda, H. *Atmos. Environ.* **1990**, *24A*, 1443–1450.
(7) Kawamura, K.; Gagosian, R. B. *Naturwissenschaften* **1990**, *77*, 25–27.
(8) Lamar, W. L.; Goerlitz, D. F. Organic Acids in Naturally Colored Surface Waters. *U.S. Geol. Surv. Water-Supply Pap.* **1966**, *No. 1817-A*.
(9) Fox, T. R.; Comerford, N. B. *Soil Sci. Am. J.* **1990**, *54*, 1139–1144.
(10) Faust, B. C. In *Aquatic and Surface Photochemistry*; Helz, G., Zepp, R. G., Crosby, D., Eds.; Lewis: Chelsea, MI, 1993, in press.
(11) Miles, C. J.; Brezonik, P. L. *Environ. Sci. Technol.* **1981**, *15*, 1089–1095.
(12) Parker, C. A. *Trans. Faraday Soc.* **1954**, *50*, 1213–1221.
(13) Parker, C. A.; Hatchard, C. G. *J. Phys. Chem.* **1959**, *63*, 22–26.
(14) Balzani, V.; Carassiti, V. *Photochemistry of Coordination Compounds*; Academic: New York, 1970; Chapter 10, pp 172–174.
(15) Cooper, G. D.; DeGraff, B. A. *J. Phys. Chem.* **1971**, *75*, 2897–2902.
(16) Cooper, G. D.; DeGraff, B. A. *J. Phys. Chem.* **1972**, *76*, 2618–2625.
(17) Zepp, R. G.; Faust, B. C.; Hoigné, J. *Environ. Sci. Technol.* **1992**, *26*, 313–319.
(18) Zuo, Y.; Hoigné, J. *Environ. Sci. Technol.* **1992**, *26*, 1014–1022.
(19) Mulazzani, Q. G.; D'Angelantonio, M.; Venturi, M.; Hoffman, M. Z.; Rodgers, M. A. J. *J. Phys. Chem.* **1986**, *90*, 5347–5352.
(20) Ross, A. B.; Neta, P. Rate Constants for Reactions of Aliphatic Carbon-Centered Radicals in Aqueous Solution. *Natl. Stand. Ref. Data Ser. (U.S. Natl. Bur. Stand.)* **1982**, *NSRDS-NBS 80*.
(21) Goldstein, S.; Czapski, G.; Cohen, H.; Meyerstein, D. *J. Am. Chem. Soc.* **1988**, *110*, 3903–3907.

(22) Smith, R. M.; Martell, A. E. *Critical Stability Constants*; Plenum: New York, 1977; Vols. 3–6.
(23) Wagman, D. D.; Evans, W. H.; Parker, V. B.; Schumm, R. H.; Halow, I.; Bailey, S. M.; Churney, K. L.; Nuttall, R. L. *J. Phys. Chem. Ref. Data* **1982**, *11* (Suppl. 2), 177.
(24) Delien, I. *Acta Chem. Scan.* **1977**, *A31*, 473–479.
(25) Field, T. B.; McCourt, J. L.; McBryde, W. A. E. *Can. J. Chem.* **1974**, *52*, 3119–3124.
(26) Hamm, R. E.; Shull, S. M.; Gant, D. M. *J. Am. Chem. Soc.* **1954**, *76*, 2111.
(27) Amico, P.; Daniele, P. G.; Cucinotta, V.; Rizzarelli, E.; Sammartano, S. *Inorg. Chim. Acta* **1979**, *36*, 1–7.
(28) Feitknecht, W.; Schindler, P. *Solubility Constants of Metal Oxides, Metal Hydroxides and Metal Hydroxide Salts in Aqueous Solutions*; Butterworth: London, 1963.
(29) Stumm, W.; Morgan, J. J. *Aquatic Chemistry*; Wiley: New York, 1981; p 135.
(30) Hatchard, C. G.; Parker, C. A. *Proc. R. Soc. London, Ser. A* **1956**, *235*, 518–536.
(31) Lever, A. B. P. *J. Chem. Educ.* **1974**, *51*, 612–616.
(32) Zepp, R. G., U.S. Environmental Protection Agency, 1988, unpublished results.
(33) Rush, J. D.; Maskos, Z.; Koppenol, W. H. *Methods Enzymol.* **1990**, *186*, 148–156.
(34) Moffett, J. W.; Zika, R. G. *Environ. Sci. Technol.* **1987**, *21*, 804–810.
(35) Faust, B. C.; Hoigné, J. *Atmos. Environ.* **1990**, *1*, 79–89.

Received for review March 4, 1993. Revised manuscript received June 21, 1993. Accepted June 22, 1993.[⊗]

[⊗] Abstract published in *Advance ACS Abstracts*, August 15, 1993.